Silver nanoparticles of variable morphology synthesized in aqueous foams as novel templates

SAIKAT MANDAL, SUJATHA K ARUMUGAM, RENU PASRICHA and MURALI SASTRY*

Materials Chemistry Division, National Chemical Laboratory, Pune 411 008, India

Abstract. In this paper, we describe the synthesis of silver nanocrystals within aqueous foams as a template. More specifically, we show that aqueous Ag$^+$ ions may be electrostatically complexed with the anionic surfactants aerosol OT (sodium *bis*-2-ethylhexyl-sulfosuccinate, (AOT) and sodium dodecyl sulphate (SDS)) in a highly stable liquid foam. After drainage of the foam, the silver ions are reduced *in situ* by introducing sodium borohydride into the foam by capillary flow. This leads to the formation of silver nanoparticles of spherical, tape- and sheet-like morphology in the foam. The structure of the foam is extremely complex and presents reaction sites of different spatial extent. The differences in foam reaction–site geometry are believed to be responsible for the morphology variation in the silver nanoparticles observed. The silver nanoparticles are observed to be extremely stable in solution suggesting that the AOT or SDS molecules stabilize them. This approach appears promising for application in large-scale synthesis of nanoparticles and may be readily extended to other chemical compositions.

Keywords. Composites; chemical synthesis; intercalation; foam; nanoparticles.

1. Introduction

The size and shape-dependent properties of nanomaterials provide a challenge to synthetic chemists for obtaining highly functional advanced materials. It is well known that the shape and size of inorganic nanocrystals control their widely varying electrical, optical and catalytic properties (Alivisatos 1996; Huang and Murray 2001; Kamat 2002). El-Sayed (2001) has shown that cubic platinum nanoparticles with their surfaces bound by {100} facets prefer to adsorb hydrogen molecules, while carbon monoxide tends to interact strongly with buckyball-shaped platinum nanoparticles bound by {210} facets. Consequently, one of the emerging challenges in materials synthesis is achieving control over the morphology of nanocrystals. One can achieve shape control by the use of a static template to enhance the growth rate of one crystallographic face over another. For example, two-dimensional films of GaAs are obtained when there is favourable epitaxy on a substrate (Cho 1999) as is the case of calcite growth on carboxyl-terminated lipid bilayers (Berman 1995). Hu and co-workers have synthesized one-dimensional Si nanowires by the vapour–liquid–solid growth mechanism using a catalyst (Hu *et al* 1999). There are also many demonstrated cases of anisotropic inorganic nanocrystal growth in liquid media. Swami and co-workers have recently

demonstrated the spontaneous reduction of chloroaurate ions present in the aqueous subphase by Langmuir monolayers of hexadecylamine molecules that resulted in the formation of highly oriented, flat gold nanosheets/nanoribbons bound to the monolayer (Swami *et al* 2003). Structured reaction media such as regular or inverse micelles (Qi *et al* 1997; Tanori and Pileni 1997; Li *et al* 1999; Chen *et al* 2000) as well as electrochemical methods (Yu *et al* 1997; Chang *et al* 1999) have also been used successfully for the synthesis of anisotropic gold nanoparticles. Recently, Pastoriza-Santos and Liz-Marzan (2002) have shown the synthesis of silver nanoprisms in dimethylformamide using a polymeric stabilizer. Silver nanodisks have also been formed by sonicating silver ions and hydrazine dissolved in reverse micelles consisting of *di*(2-ethyl-hexyl)sulfosuccinate (AOT), isooctane and water (Maillard *et al* 2002). Yener *et al* (2002) have reported a process for making nanosized silver platelets using soft templates such as the octylamine–water bilayer system. A micellar system involving cetyltrimethylammonium bromide (CTAB) was adopted to generate triangular nanoplates (with highly truncated corners) and circular nanodisks of silver through a seed-mediated growth process (Chen and Carroll 2002). Maillard and co-workers have recently demonstrated the synthesis of silver nanodisks by varying the ratio of surfactant AOT to the reducing agent (hydrazine) in reverse micelle solution made of Ag(AOT) and Na(AOT) in water and isooctane mixtures (Maillard *et al* 2002, 2003). Shape transformations have

*Author for correspondence (m.sastry@ncl.res.in)

also been the focus of recent studies. Sun *et al* (2003) have reported the transformation of silver nanospheres into nanobelts and triangular nanoplates through a thermal process. Nanorods of silver (Chung *et al* 1998; Jana *et al* 2001), gold (Esumi *et al* 1995; Brown *et al* 2000; Johnson *et al* 2002), CdSe (Peng *et al* 2000), tungsten sulfide (Nikitenko *et al* 2002), and nanoprisms of silver (Jin *et al* 2001), gold (Malikova *et al* 2002), and CdS (Pinna *et al* 2001) are some of the other interesting nanocrystalline shapes that may now be routinely synthesized in the laboratory. Insofar as metal nanowires/rods are concerned, experimental protocols based on templating (van der Zande *et al* 1997; Nicewarner-Pena *et al* 2001), photochemistry (Esumi *et al* 1995), seeding (Murphy and Jana 2002; Sun and Xia 2002) and electrochemistry (Yu *et al* 1997; Chang *et al* 1999) have been developed.

An exciting and hitherto considerably underexploited dynamic biomimetic template for crystal growth is foam lamellae (Chen *et al* 1998). Chen *et al* (1998) showed that stabilizing surfactants at the air-bubble/solution interface in foams could be used as nucleation centres for the growth of glycine and CaCO$_3$ crystals. Liquid foams essentially consist of very high density of gas bubbles dispersed in a liquid. The bubbles are stabilized in the liquid matrix by surfactants that adsorb at the gas/liquid interface and are separated by a thin layer of water that, depending on the

drainage of the foam etc can approach nanoscale thicknesses. We recognize that the structure of the foam thus consists of bubbles and bilayers of surfactants that are rather similar to two Langmuir monolayers separated by a water channel (scheme 1). By using ionizable surfactants in the foam, it should be possible to electrostatically attach metal ions to the surfactants and thereafter, carry out interesting chemistry to yield a large number of materials over a range of chemical compositions formed directly in the foam.

In this article we describe a novel, simple procedure for the synthesis of anisotropic silver nanoparticles in aqueous foams stabilized by the anionic surfactants (AOT) and sodium dodecyl sulphate (SDS). This is accomplished in a two-step process involving the electrostatic binding of Ag$^+$ ions with AOT/SDS molecules at the air-bubble solution interface in the foam followed by reaction with NaBH$_4$ solution in the final step. The silver ions are reduced in the foam that acts as a template and results in the formation of silver nanoparticles of different morphologies that we believe originate in structurally different regions of the foam (scheme 1). Our interest in developing a foam-based method for the synthesis of nanomaterials stems from the fact that the large internal surface area of the foam can be utilized to synthesize large amounts of nanomaterials in a single step and thus
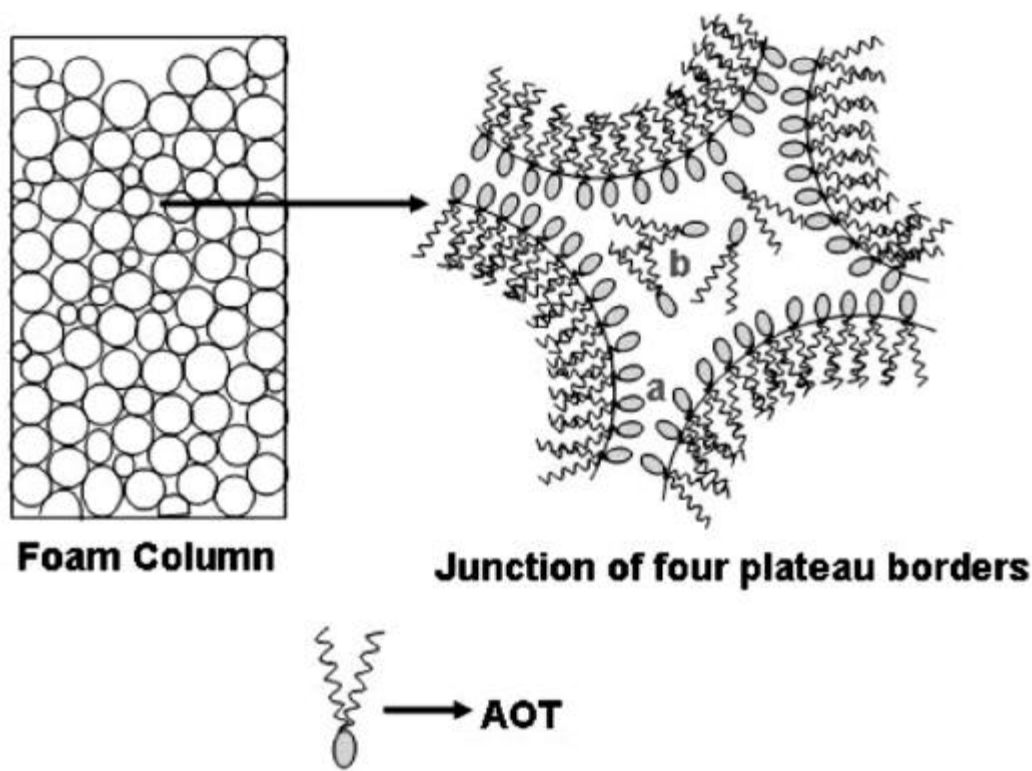
Scheme 1. Cartoon showing different regions in the foam believed to be involved in the synthesis of silver nanocrystals of variable shape. The regions 'a' and 'b' are described in the text.

provide a suitable method for scale-up. For example, there is a growing demand for large-scale production of $CaCO_3$ nanoparticles for application in polymer, paper and cosmetics industries where such foam-based methods could be important.

2. Experimental

2.1 *Chemicals*

Silver sulphate (Ag_2SO_4), aerosol OT (sodium *bis*-2-ethyl-hexyl-sulfosuccinate, AOT), sodium dodecyl sulphate (SDS) and sodium borohydride ($NaBH_4$) were obtained from Aldrich Chemicals and used as-received.

2.2 *Preparation of silver nanocrystals in aqueous AOT/SDS foam*

In a typical experiment, a rectangular column of 50 cm height and a square base of 10×10 cm^2 with sintered ceramic discs embedded in it were used for generation of the foam. An aqueous mixture of 100 ml of 5×10^{-3} M silver sulphate solution and 100 ml of 5×10^{-3} M AOT was taken in the rectangular column and the foam built up by injecting air at a pressure of 1–5 psi through a porous ceramic disc fixed to the bottom of the foam column. Stable foams of 40 cm height and with bubble size of 1 mm could routinely be obtained. After carefully draining out the excess aqueous AOT + Ag_2SO_4 solution, the silver ions in the foam were subjected to reduction by capillary flow of sodium borohydride solution into the foam. As the silver ions were reduced and nanoparticle formation progressed, the foam changed to a yellowish-brown colour and gradually collapsed. The collapsed foam solution containing silver nanoparticles was collected through an outlet provided at the bottom of the column (sample 1). This solution (sample 1) was then subjected to centrifugation at 5000 rpm for 30 min following which the pellet (sample 2) and supernatant (sample 3) were separated and characterized by different techniques. Please note that sample 2 for further analysis was prepared by redispersing the silver nanoparticle pellet in 10 ml of water. To understand the effect of foam structures on the morphological differences of silver nanoparticles, we have repeated the experiment using SDS instead of AOT as the foam-stabilizing surfactant. The experiments with the SDS foam are identical to that for AOT. The silver nanoparticle foam solution in this case is designated as sample 4.

2.3 *UV-vis spectroscopic studies*

The optical properties of AOT and SDS-capped silver nanoparticle solutions (samples 1–4) were monitored on

a Hewlett-Packard diode array spectrophotometer (model HP-8452) operated at a resolution of 2 nm.

2.4 *X-ray diffraction measurements*

X-ray diffraction (XRD) analysis of drop-coated films on glass substrates from the AOT-capped silver nanoparticles in sample 1 was carried out on a Phillips PW1830 instrument operating at 40 kV and a current of 30 mA with CuK$_a$ radiation.

2.5 *Fourier transform infrared (FTIR) spectroscopy measurements*

FTIR spectra were recorded from drop-coated films of silver nanoparticles in sample 1 deposited on a Si (111) substrate on a Perkin Elmer Spectrum-One Spectrometer operated in the diffuse reflectance mode at a resolution of 4 cm^{-1}. The spectrum of pure AOT was also recorded for comparison.

2.6 *Transmission electron microscopy (TEM) measurements*

TEM measurements were performed on a JEOL model 1200 EX instrument operated at an accelerating voltage of 120 kV. Samples for TEM studies were prepared by placing drops of the silver nanoparticle solutions in samples 1–4 on carbon-coated TEM grids. The films on the TEM grids were allowed to dry in air for 2 min following which the extra solution was removed using a blotting paper.

3. Results and discussion

Figure 1A shows the UV-vis spectra of the AOT-capped silver nanoparticle solutions in samples 1–3 (corresponding to curves 1, 2 and 3, respectively) and from the SDS-capped silver nanoparticle solution in sample 4 (curve 4, dotted line). The inset of this figure shows pictures of test tubes (labeled 1–4) that correspond to the silver nanoparticle solutions in samples 1–4, respectively. The yellow to yellowish-brown colours observed in different solutions are symptomatic of the presence of silver nanoparticles in the solutions. Strong absorption bands are observed to occur at ~ 400 nm for all the samples (curves 1–4, figure 1A). This characteristic resonance corresponds to excitation of surface plasmon vibrations in the silver nanoparticles and is responsible for the striking colours of the different samples (inset, figure 1A). In addition to the sharp absorption band at 400 nm, samples 1 and 2 (curves 1 and 2, respectively, figure 1A) also show the presence of an additional absorption band at higher wavelengths (~ 540 nm). There are two possible explanations for this

long-wavelength band. One is that the AOT-stabilized silver nanoparticles are in a highly aggregated state leading to coupling of the plasmon vibrations between neighbouring particles (Taleb *et al* 1998; Tan *et al* 2002). The other possibility is that the silver nanoparticles are anisotropic in shape (Jin *et al* 2003). In contrast, the silver nanoparticles produced in the SDS foam (curve 4) does not show any obvious broadening of the plasmon vibration band or an additional band at higher wavelengths. The different silver nanoparticle solutions were extremely stable in time with no evidence of aggregation of the particles even after weeks of storage. This indicates significant stabilization of the particles, presumably through surface capping of the silver nanoparticles by the surfactants, AOT/SDS. The differences in the optical properties of the nanoparticle solutions 1–4, particularly between samples 2 and 3, clearly indicate significant variation in either the state of aggregation of the silver nanoparticles or the shape of the nanoparticles. This issue will be addressed during analysis of TEM micrographs. Figure 1B shows the XRD pattern recorded from a drop-cast film of the silver nanoparticles in sample 1. A number of strong Bragg reflections can be seen which correspond to the (111), (200), (220), (311) reflections of *fcc* silver. The XRD results thus show that the silver nanoparticles formed within the foam are crystalline. Similar diffraction patterns were recorded from samples 2–4 and have not been shown for brevity.

Figure 2 shows the FTIR spectra in the region 1000–3100 cm^{-1} recorded from solution-cast films of pure AOT (curve 1) and AOT-capped silver nanocrystals obtained in sample 1 (curve 2). The methylene symmetric and antisymmetric stretching vibrations in both samples are observed to occur close to 2850 and 2920 cm^{-1}, respectively. Absorption bands are also seen at 1054 and 1736 cm^{-1} in the case of pure AOT (curve 1). The band at 1054 cm^{-1} is assigned to the S=O stretching vibration of the sulfonate group present in the AOT molecules and the band at 1736 cm^{-1} is due to carbonyl stretch vibrations in the AOT molecules. These bands are shifted to 1062 cm^{-1} and 1749 cm^{-1} in the AOT-capped silver nanoparticle film (curve 2) and indicate that surfactant is bound to the silver nanoparticle surface through the hydrophilic sulfonate/carboxylic acid groups. It is also possible that AOT (and indeed SDS) caps the silver nanoparticles via an interdigitated bilayer. At this stage, we are unable to unequivocally make a statement on whether the surfactant exists as a monolayer or bilayer on the surface of the silver nanoparticles.

Figures 3A and B show representative TEM micrographs recorded at different magnifications from a drop-cast film of AOT-capped silver nanoparticles in sample 1. Highly anisotropic silver particles with an overall tape-like morphology are seen that co-exist with a small percentage of nearly spherical particles. The higher magnification image (figure 3B) shows the morphology of one
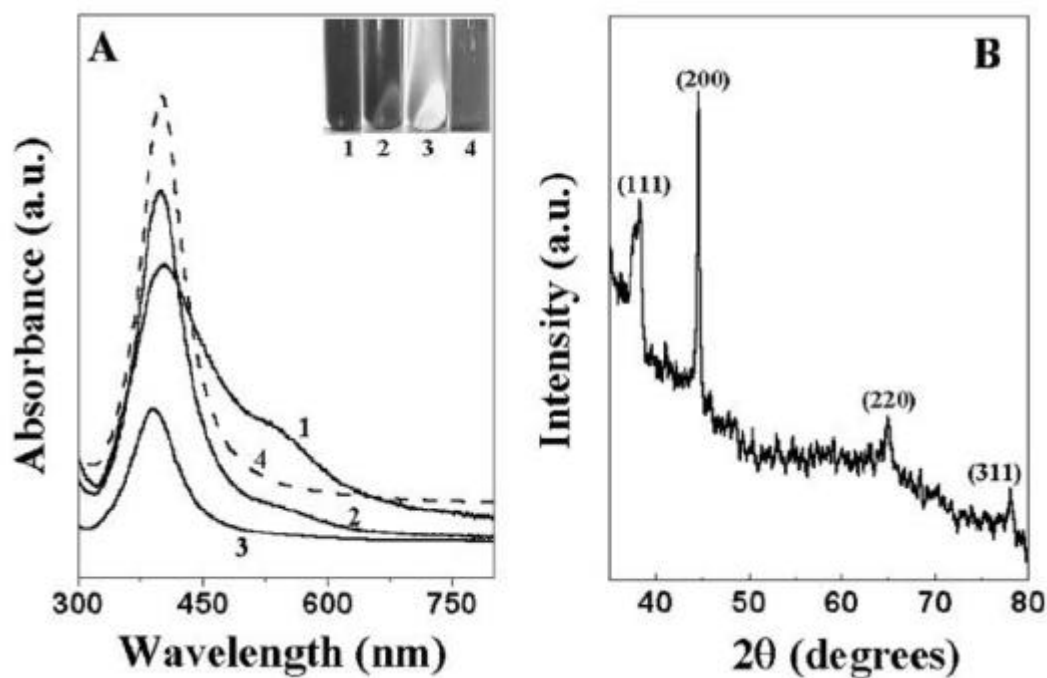
Figure 1. **A.** UV-vis spectra recorded from sample 1 (curve 1), sample 2 after redispersion in water (curve 2), sample 3 (curve 3) and sample 4 (curve 4, dotted line). The inset shows pictures of test tubes of silver nanoparticle solutions in samples 1–4 and **B.** XRD pattern recorded from a drop-coated film of sample 1 on glass substrate.

tape-like silver nanoparticle aggregate in greater detail. The width of the tapes is non-uniform and varies from 5–20 nm. From the TEM measurements, it is clear that the additional absorption band at 540 nm in the UV-vis spectrum of the AOT-capped silver nanoparticles in sample 1 (figure 1A, curve 1) can be attributed to the flat, anisotropic structure of the nanoparticles and not to aggregation of the particles. The inset of figure 3B shows the selected
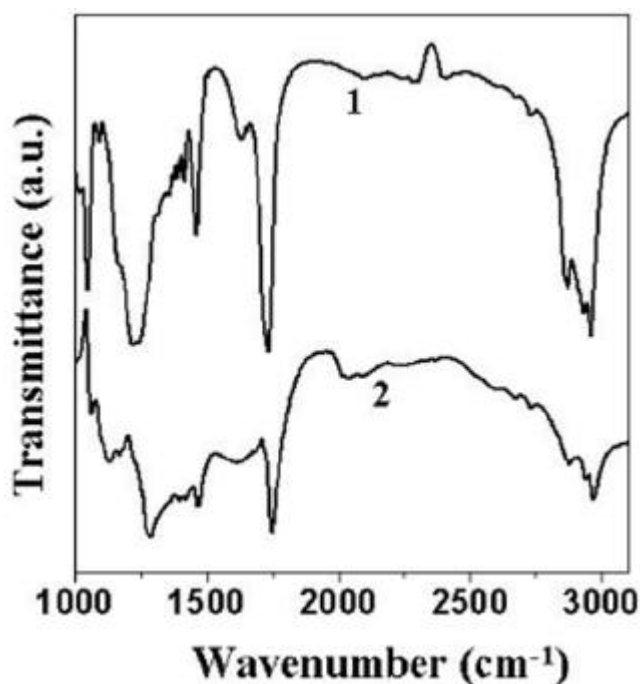
Figure 2. FTIR spectra recorded from a drop-coated film of pure AOT (curve 1) and sample 1 on Si (111) substrates (curve 2).

area diffraction (SAED) pattern recorded from the silver nanotapes shown in figure 3B. The sharp spots in the SAED pattern indicate that the flat silver nanotapes are single crystalline in nature. The diffraction spots marked by circles correspond to the (111) reflections while those marked by squares arise from the (200) reflections from *fcc* silver.

Figures 4A and B show representative TEM micrographs recorded from a drop-cast film of silver nanoparticles in sample 2. To recollect, this sample is prepared by centrifugation of the as-prepared AOT-capped silver nanoparticles in the foam followed by redispersion of the pellet in water. Highly irregular and extremely flat silver nanosheets/flakes can be seen in these TEM micrographs. That these silver nanosheets are extremely thin is indicated by the fact that buckling of the particles is observed as strain features in the nanosheets. A region where the particles overlap leads to increased contrast and is an additional indication that the silver nanosheets are quite thin. There was no evidence of the presence of spherical silver nanoparticles in this sample indicating that the centrifugation was successful in removing the spherical structures seen in the as-prepared AOT-capped silver nanoparticles (figure 3). The silver nanosheets vary in size from 20–90 nm and appear to be made of triangular silver nanostructures. The inset of figure 4B shows the SAED pattern recorded from the silver nanosheets shown in figure 4B. It is clear from the SAED pattern that the silver nanosheets are single crystalline and have been indexed on the basis of *fcc* structure of silver. The diffraction spots marked by circles correspond to the (111) reflections while those circumscribed by squares are due to (200) reflections. While there are a large number of reports on the synthesis of silver nanodisks and triangles
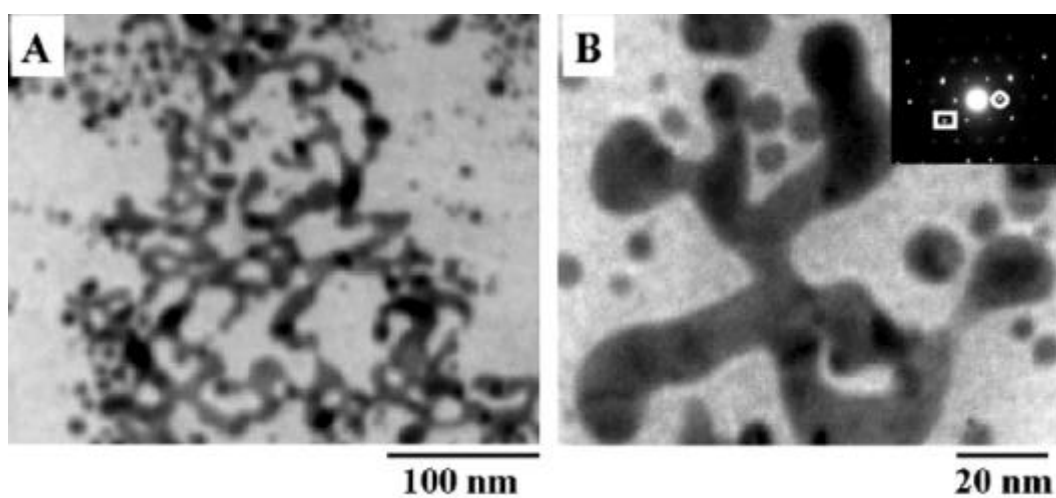
Figure 3. A and B. Representative TEM micrographs recorded at different magnifications from drop-cast films of silver nanoparticles from sample 1. The inset of **B** shows the selected area electron diffraction (SAED) pattern recorded from the flat-silver nanotapes in the figure.

(introductory section), to the best of our knowledge there are no reports on the synthesis of single crystalline silver nanosheets in the manner observed in our present study.

Figures 5A and B show representative TEM micrographs recorded at different magnifications from a drop-cast film of AOT-capped silver nanoparticles in sample 3 (the supernatant obtained by centrifugation of sample 1). A significant percentage of predominantly spherical silver nanoparticles are seen in these TEM micrographs. The spherical particles are reasonably uniform and range in size from 5–40 nm. Thus, centrifugation leads to separation of the relatively lighter spherical silver nanoparticles in the supernatant while the heavier nanotapes/nanosheets accumulate in the pellet (figure 4).

Figures 6A and B show representative TEM micrographs recorded from a drop-cast film of SDS-capped silver nanoparticles in sample 4. Highly anisotropic silver particles with plate-like morphology are seen that co-exist with a small percentage of nearly spherical particles. In gross detail, the nature of silver nanoparticles formed in the SDS foam is similar to that of the AOT foam (figures 3–5) suggesting that the templating mechanism leading to the morphology variation is identical in both cases. On a finer scale, the silver nanoparticles in sample 4 appear to be thicker than those obtained in the AOT foam. While both AOT and SDS are anionic, AOT is a twin-tailed surfactant and this may contribute to variation in the fine structure of the foam. These aspects will be studied in greater detail in forthcoming reports. The inset of figure 6A shows the SAED pattern recorded from silver nanoparticles as shown in figure 6A. The silver nanostructures are clearly polycrystalline. The diffraction rings in the figure could be indexed on the basis of the *fcc* structure of silver.
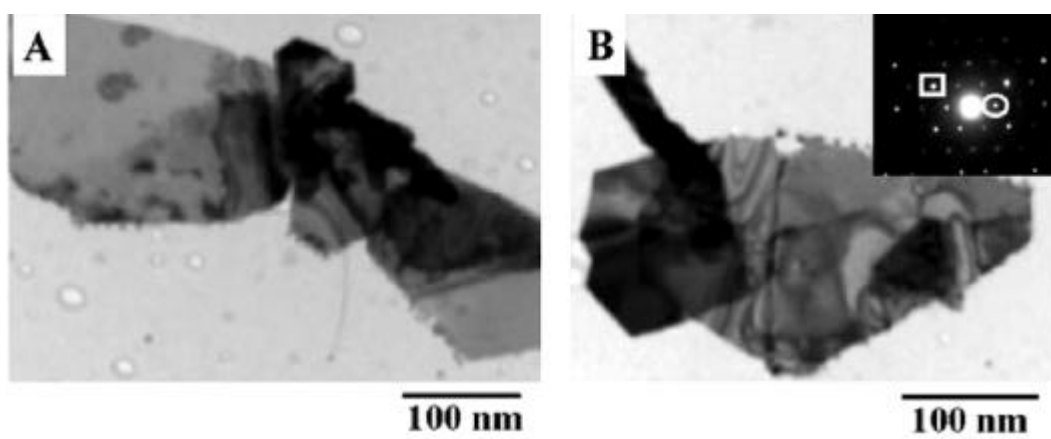
Figure 4. A and B. Representative TEM micrographs from drop-cast films from sample 2 after redispersion in water. The inset of **B** shows the selected area electron diffraction (SAED) pattern recorded from the silver nanosheets in this figure.
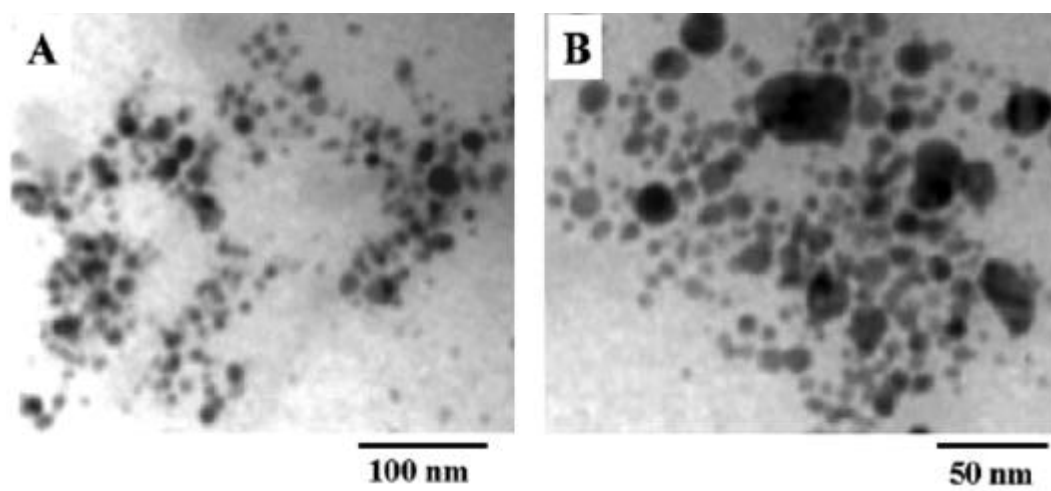
Figure 5. A and B. Representative TEM micrographs recorded at different magnifications from drop-cast films of sample 3.
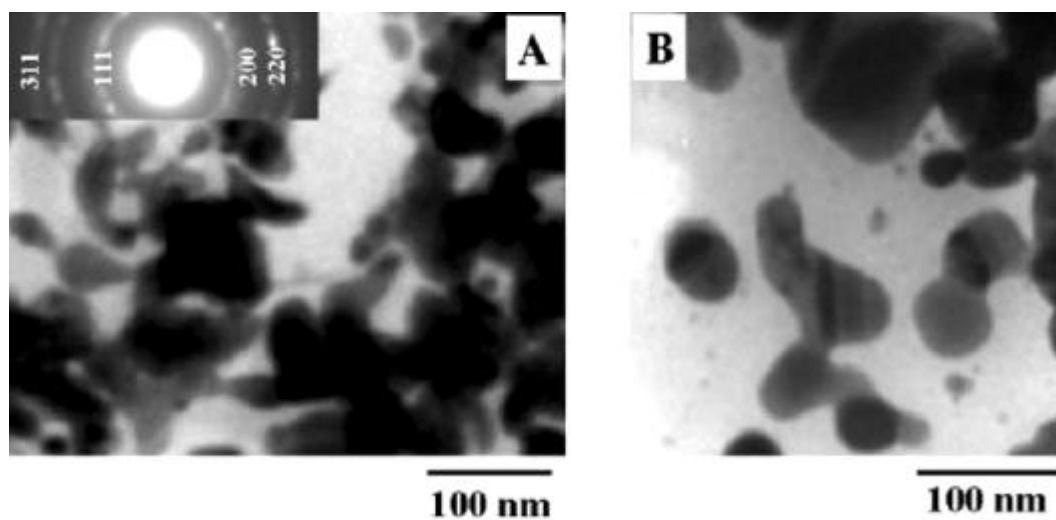
Figure 6. A and B. Representative TEM micrographs recorded from drop-cast films of silver nanoparticles in sample 4. The inset of A shows the selected area electron diffraction (SAED) pattern recorded from the flat-silver nanoplates in this figure.

In scheme 1 we illustrate a possible mechanism operative in the foam that could explain the differences in morphology of the silver nanoparticles grown. The liquid lamellae between bubbles in the foam may be considered to consist of two Langmuir monolayers of AOT electrostatically complexed with Ag^+ ions and therefore, the silver ions are amenable to borohydride reduction at only the interface. Region 'a' in scheme 1 shows the liquid lamellae within the plateau borders of the foam wherein the thickness of this region is very small. It is likely that this is the nanoreactor where formation of flat silver nanoplates by borohydride reduction of Ag^+ ions occurs. Region 'b' shows the junction of four plateau borders where the reaction space for formation of silver nanoparticles is more extended and isotropic. We believe that the spherical silver nanoparticles form in this region of the foam. However, we caution that much work is required before a full appreciation of the capabilities of the nanoreactors in the foams is achieved. The schematic illustrates the case of silver ion binding in AOT-stabilized foams but in gross detail, is expected to be similar for the foams stabilized with SDS molecules as well.

4. Conclusions

The formation of silver nanocrystals in liquid foams stabilized by the surfactants, AOT and SDS, has been described. The process of silver ion entrapment in the foam and their *in situ* reduction results in the formation of silver nanostructures of variable morphology in the foam. The silver nanoparticle morphology varies from spherical to flat plates/tapes and simple centrifugation enables separation of the different shapes. This morphology variation in the silver nanocrystals is believed to occur due to differences in the structure of the foam, which varies from highly anisotropic (liquid lamellae between bubbles) to extended and isotropic (junction between plateau borders). A combination of extremely large interfacial templating area provided by the liquid lamellae in foams and the dynamic nature of the foam bubbles makes this method potentially exciting for the large-scale synthesis of other inorganic materials (nanomaterials) and minerals and are currently being attempted.

References

Alivisatos A P 1996 *Science* **271** 933
Berman A D, Ahn J, Lio A, Salmeron M, Reichert A and Charych D 1995 *Science* **269** 515
Brown K R, Walter D G and Natan M J 2000 *Chem. Mater.* **12** 306
Chang S S, Shih C W, Chen C D, Lai W C and Wang C R C 1999 *Langmuir* **15** 701
Chen B-D, Cilliers J J, Davey R J, Garside J and Woodburn E T 1998 *J. Am. Chem. Soc.* **120** 1625
Chen C C, Chao C Y and Lang Z H 2000 *Chem. Mater.* **12** 1516
Chen S and Carroll D L 2002 *Nano Lett.* **2** 1003
Cho A Y 1999 *J. Cryst. Growth* **202** 1
Chung S-W, Markovich G and Heath J R 1998 *J. Phys. Chem.* **B102** 6685

El-Sayed M A 2001 *Acc. Chem. Res.* **34** 257

Esumi K, Matsuhisa K and Torigoe K 1995 *Langmuir* **11** 3285

Huang T and Murray R W 2001 *J. Phys. Chem.* **B105** 12498

Hu J T, Odom T W and Lieber C M 1999 *Acc. Chem. Res.* **32** 435

Jana N R, Gearhart L and Murphy C J 2001 *Chem. Commun.* 617

Jin R, Cao Y, Mirkin C A, Kelly K L, Schatz G C and Zheng J G 2001 *Science* **294** 1901

Jin R, Charles Cao Y, Hao E, Gabriella S M, George C S and Mirkin C A 2003 *Nature* **425** 487

Johnson C J, Dujardin E, Davis S A, Murphy C J and Mann S 2002 *J. Mater. Chem.* **12** 1765

Kamat P V 2002 *J. Phys. Chem.* **B106** 7729

Li M, Schnablegger H and Mann S 1999 *Nature* **402** 393

Maillard M, Giorgio S and Pileni M-P 2002 *Adv. Mater.* **14** 1084

Maillard M, Giorgio S and Pileni M P 2003 *J. Phys. Chem.* **B107** 2466

Malikova N, Pastoriza-Santos I, Schierhorn M, Kotov N A and Liz-Marzan L M 2002 *Langmuir* **18** 3694

Murphy C J and Jana N R 2002 *Adv. Mater.* **14** 80

Nicewarner-Pena S R *et al* 2001 *Science* **294** 137

Nikitenko S I, Koltypin Y, Mastai Y, Koltypin M and Gedanken A 2002 *J. Mater. Chem.* **12** 1450

Pastoriza-Santos I and Liz-Marzan L M 2002 *Nano Lett.* **2** 903

Peng X, Manna L, Yang W, Wickham J, Scher E, Kadanavich A and Alivisatos A P 2000 *Nature* **404** 59

Pinna N, Weiss K, Urban J and Pileni M-P 2001 *Adv. Mater.* **13** 261

Qi L M, Ma J M, Cheng H M and Zhao Z G 1997 *J. Phys. Chem.* **B101** 3460

Sun Y G and Xia Y N 2002 *Adv. Mater.* **14** 833

Sun Y, Mayers B and Xia Y 2003 *Nano Lett.* **3** 675

Swami A, Kumar A, Selvakannan P R, Mandal S, Pasricha R and Sastry M 2003 *Chem. Mater.* **15** 17

Taleb A, Petit C and Pileni M P 1998 *J. Phys. Chem.* **B102** 2214

Tanori J and Pileni M P 1997 *Langmuir* **13** 639

Tan Y, Jiang L, Li Y and Zhu D 2002 *J. Phys. Chem.* **B106** 3131

van der Zande B M I, Bohmer M R, Fokkink L G J and Schonenberger C 1997 *J. Phys. Chem.* **B101** 852

Yener D O, Sindel J, Randall C A and Adair J H 2002 *Langmuir* **18** 8692

Yu Y Y, Chang S, Lee C J and Wang C R C 1997 *J. Phys. Chem.* **B101** 6661